ORIGINAL RESEARCH

Altered Macrophage Function Associated with Crystalline Lung Inflammation in Acid Sphingomyelinase Deficiency

Joanna M. Poczobutt[1]*, Andrew M. Mikosz[1]*, Christophe Poirier[2†], Erica L. Beatman[1], Karina A. Serban[1,3], Fabienne Gally[1,3], Danting Cao[1], Alexandra L. McCubbrey[1,3], Christina F. Cornell[1], Kelly S. Schweitzer[1,3], Evgeny V. Berdyshev[1], Irina A. Bronova[1], François Paris[4,5], and Irina Petrache[1,2,3]

[1]National Jewish Health, Denver, Colorado; [2]Indiana University, Indianapolis, Indiana; [3]University of Colorado, Denver, Colorado; [4]Institut de Cancérologie de l'Ouest, Saint-Herblain, France; and [5]Le Regional Center for Research in Cancerology and Immunology Nantes/Angers, Université de Nantes, Nantes, France

ORCID IDs: 0000-0002-9372-3034 (K.A.S.); 0000-0003-0503-7411 (F.G.); 0000-0003-1094-2600 (I.P.).

Abstract

Deficiency of ASM (acid sphingomyelinase) causes the lysosomal storage Niemann-Pick disease (NPD). Patients with NPD type B may develop progressive interstitial lung disease with frequent respiratory infections. Although several investigations using the ASM-deficient (ASMKO) mouse NPD model revealed inflammation and foamy macrophages, there is little insight into the pathogenesis of NPD-associated lung disease. Using ASMKO mice, we report that ASM deficiency is associated with a complex inflammatory phenotype characterized by marked accumulation of monocyte-derived $CD11b^+$ macrophages and expansion of airspace/alveolar $CD11c^+$ $CD11b^-$ macrophages, both with increased size, granularity, and foaminess. Both the alternative and classical pathways were activated, with decreased *in situ* phagocytosis of opsonized (Fc-coated) targets, preserved clearance of apoptotic cells (efferocytosis), secretion of Th2 cytokines, increased $CD11c^+$/$CD11b^+$ cells, and more than a twofold increase in lung and plasma proinflammatory cytokines. Macrophages, neutrophils, eosinophils, and noninflammatory lung cells of ASMKO lungs also exhibited marked accumulation of chitinase-like protein Ym1/2, which formed large eosinophilic polygonal Charcot-Leyden–like crystals. In addition to providing insight into novel features of lung inflammation that may be associated with NPD, our report provides a novel connection between ASM and the development of crystal-associated lung inflammation with alterations in macrophage biology.

Keywords: sphingomyelinase; macrophages; chitinases; inflammation; neutrophils

Clinical Relevance

Using a model of the lysosomal storage Niemann-Pick disease, the mouse knockout for acid sphingomyelinase, we found a lung crystalopathy with Ym1 protein accumulation analogous to Charcot-Leyden crystals. This was associated with markers of lung and systemic Th2 and Th1 inflammation and with marked complex macrophage inflammatory activation with decreased Fc-mediated phagocytosis but preserved apoptotic cell clearance. Our findings may provide insight into the pathogenesis of respiratory dysfunction in Niemann-Pick disease type B, which is driven by progressive interstitial lung disease and frequent respiratory infections.

(Received in original form June 2, 2020; accepted in final form February 12, 2021)

*These authors contributed equally to this work.

†Deceased.

Supported by U.S. National Institutes of Health grant RO1HL077328 (I.P.) and RO1HL141264 (F.G.).

Author Contributions: Conception and design of the study: I.P. Performed the experiments: J.M.P., A.M.M., C.P., E.L.B., K.A.S., F.G., D.C., A.L.M., C.F.C., K.S.S., E.V.B., I.A.B., and F.P. Analysis and interpretation of the data: J.M.P., A.M.M., E.L.B., K.A.S., F.G., D.C., A.L.M., C.F.C., K.S.S., E.V.B., I.A.B., F.P., and I.P. Manuscript draft and revision: J.M.P. and I.P. Manuscript contribution: A.M.M., F.G., A.L.M., C.F.C., and E.V.B. All authors edited and approved the final version of the manuscript.

Correspondence and requests for reprints should be addressed to Irina Petrache, M.D., National Jewish Health, 1400 Jackson Street, Denver, CO 80206. E-mail: petrachei@njhealth.org.

This article has a data supplement, which is accessible from this issue's table of contents at www.atsjournals.org.

Am J Respir Cell Mol Biol Vol 64, Iss 5, pp 629–640, May 2021

Originally Published in Press as DOI: 10.1165/rcmb.2020-0229OC on March 4, 2021
Internet address: www.atsjournals.org

ASM (acid sphingomyelinase; encoded by *SMPD1*) is a ubiquitous enzyme that, by hydrolyzing sphingomyelin to ceramide, plays an essential role in the sphingolipid metabolism. Genetic deficiency of ASM causes Niemann-Pick disease (NPD), a lysosomal lipid storage disorder with an early onset of progressive neurodegeneration culminating in death during childhood (NPD type A) or a later onset that causes limited neuropathy but may involve multiple organs (NPD type B). Patients with NPD type B may manifest a progressive interstitial lung disease with frequent respiratory infections (1–3). The mechanism of lung disease in NPD remains poorly understood. The lungs of patients with NPD harbor foamy lipid-laden macrophages in multiple compartments, including airspaces, walls of alveoli and airways, and pleura (1, 2, 4, 5). A similar accumulation of macrophages, together with increased inflammation, was described in the lungs of transgenic ASM-deficient mice (*Smpd1*$^{-/-}$ or ASMKO), an established model of NPD (6–8). However, it remains unknown what types of macrophages accumulate in NPD lungs and what their functional status is.

Lung macrophages play an important role in the innate immune responses, tissue remodeling, and resolution of inflammation. To exert these that require proper endosomal and lysosomal function. Whereas the secreted form of ASM (9) is rapidly activated at the plasma membrane in response to cellular stress (10–13) and triggers apoptosis (10, 14–16), the lysosomal ASM has been involved in the regulation of endocytosis, phagocytosis, and autophagy (12, 13, 17, 18). It is therefore expected that ASM plays an important role in lung macrophage function during both homeostatic conditions and acute and chronic lung diseases. However, which macrophage subset will be regulated by ASM is not readily predictable. Resident alveolar (airspace) macrophages (CD11c^{+}/CD11b^{-} cells) are the predominant immune cells in the airspace during homeostatic conditions. Expressing mannose receptor and Ym1 at baseline, previously considered "M2 markers" (19–21), resident airspace macrophages play a key role in lung tissue homeostasis and in host defense, including surfactant turnover, apoptotic cell removal (efferocytosis), and phagocytosis of antibody-opsonized pathogens (22). However, their responsiveness to inflammatory stimuli is weak (21). During inflammatory conditions, monocyte-derived airspace macrophages (CD11b^{hi}) can be recruited to the airspace, often driving an increase in total macrophage numbers (23–25). Recruited macrophages are more responsive to inflammatory stimuli (21, 26). Additional macrophage subsets exist within the lung tissue and are termed "interstitial macrophages."

Using ASMKO mice, we report novel features of lung inflammation associated with ASM deficiency that implicate ASM in lung macrophage function and programming. We show that ASM deficiency increases recruitment of monocyte-derived CD11b+ macrophages in the airspaces and is associated with marked accumulation of chitinase-like protein Ym1 in the lung, forming large eosinophilic polygonal amorphous structures, which are analogous to Charcot-Leyden crystals. In addition, ASM-deficient lung macrophages are less apt at clearing opsonized (Fc-coated) targets but have a heightened ability to clear apoptotic targets.

Methods

Animal Studies

The animal studies were approved by the institutional animal care and use committees at Indiana University and at National Jewish Health. ASMKO mice, originally obtained from Dr. Edward Schuchman (Mount Sinai, New York) (7), of both sexes were studied with wild-type (WT) or heterozygous (ASM-HT) littermates when they reached at least 9 weeks of age. Lungs were processed as described (27). BAL fluid (BALF) was collected via serial lavages with PBS containing EDTA. Preparation of lung single-cell suspension used Liberase (Roche/Sigma) and filtration through a 100-μm nylon filter. Peritoneal macrophages were obtained by standard protocol (28).

Flow Cytometry

Analysis of BALF was performed using blocking antibodies CD16/CD32 (clone 93, #14–0161–85; eBioscience) and labeling with Ly6G (1A8, #127612; Biolegend), CD11b (clone M1/70, #45–0112–8; eBioscience), CD11c (clone N418, #47–0114–82; eBioscience), CD64 (clone X54–5/7.1, #558539; BD Bioscience), F4/80 (clone BM8, #25–4801–82; Invitrogen), CD45 (clone 30-F11, #564279; BD Bioscience), or Siglec F (clone E50–2440, #5652757; BD Bioscience) antibodies. Flow cytometry of lung single-cell suspension used blocking with CD16/CD32 and labeling with CD45-BUV395 (clone 30-F11, #564279; BD Bioscience), Ly6C-FITC (clone HK1.4, #128006; Biolegend), CD11b-PerCP-Cy5.5 (clone M1/70, #45–0112–82; Invitrogen), MerTK-PE (clone 2B10C42, #151505; Biolegend), SiglecF-PE-CF594, Ly6G-Pacific Blue (clone 1A8, #127612; Biolegend), Ly6G-PE-Cy7 (clone 1A8, #127617; Biolegend), CD64-AlexaFluor 647 (clone X54–5/7.1, #558539; BD Bioscience), or CD11c-APC-eFluor780 (clone N418, #47–0114–82; Invitrogen) antibodies. For intracellular staining, cells were permeabilized using FOXP3/Transcription Factor Staining Buffer Set (#00–5523–00; eBioscience) and incubated with Ym1-biotin antibody (1:100, #BAF2446; R&D) and Streptavidin-PE-Cy7 (1:500, #B300682; Biolegend) or Straptavidin-Qdot605 (1:500, #Q10103MP; Invitrogen). Analysis used the LSR II cytometer (BD Bioscience) and FlowJo. The gating strategy is shown in Figure E1.

Cytospins

Cells were counted, spun onto slides, and stained with Three-Step Stain Set (#3300; Richard Allan Scientific).

Western Blotting

Western blotting was performed with vinculin (ab18058; Abcam), LC3B (L7543; Sigma), SQSTM1/p62 (H00008878-M01; Abnova), and LAMP2 (sc-8100; Santa Cruz) antibodies. Images were taken with a ChemiDoc XRS with Image Lab software (Bio-Rad), and densitometry was performed with ImageJ.

Immunofluorescence Microscopy

Lung tissue sections were probed with Ly-6G (#127610; Biolegend), CD68 (KP1) (#ab955; Abcam), CD11b (M1/70) (#ab8878; Abcam), CD11c (3.9) (#ab11029; Abcam), or Ym1/2 (EPR15263) (#ab205490; Abcam) antibodies. Imaging was performed using a Zeiss LSM 700 confocal microscope with Zen Black version 14 software, and postimaging processing was performed with ImageJ.

Sphingolipid Measurement

Lipid quantification was performed using liquid chromatography tandem mass spectrometry, as previously described (29) on AB Sciex 6500 QTRAP triple quadrupole ion trap mass spectrometer interfaced with Agilent 1290 LC System.

Lung and Plasma Cytokine Measurement

Lysates were prepared from snap-frozen and pulverized lung. Cytokine concentrations were measured with a customized Meso Scale Discovery (MSD) Electrochemiluminescence multispot assay (V-PLEX Custom Mouse Cytokine kit, #K152A0H-1) with the following antibodies (all from MSD): IFN-γ (#D22QO), IL-1β (#D22QP), IL-4 (#D22QR), IL-5 (#D22QS), IL-6 (#D22QX), KC/GRO (#D22QT), IL-10 (#D22QV), and TNF-α (#D22QW) using the manufacturer's protocol, on an MSD instrument using Discovery Workbench Software (MSD) for analysis.

Statistical Analyses

Statistical Analyses were performed with Prism GraphPad Software as indicated. Statistical significance was set at $P < 0.05$.

Results

Lungs of ASMKO Mice Exhibit Ym1 Crystals

We analyzed hematoxylin and eosin–stained fixed lung tissue sections of homozygous *Smpd1*$^{-/-}$ mice (ASMKO) and heterozygous *Smpd1*$^{+/-}$ mice (ASM-HT) in comparison with WT littermates. Consistent with previous reports (6–8), the lungs of ASMKO mice displayed enlarged, lipid-laden macrophages, thickened alveolar walls, and overall increased cellularity in the airspaces (Figure 1A). Strikingly, lung sections revealed eosinophilic orthogonal crystals within the lungs of ASMKO mice but not in WT littermates or in ASM-HT mice (Figure 1A). Cytospins of BALF stained with Giemsa also showed the exclusive presence of large foamy macrophages, as well as orthogonal crystals, in ASMKO mice (Figure 1B). These crystals resembled eosinophilic crystals formed by the Ym1 protein (chitinase 3-like 3), which have been reported in several mouse models (30–32) but, to our knowledge, not previously described in ASM deficiency.

We noted that this phenomenon was not exclusively limited to the lung because peritoneal lavage fluid also contained crystals (Figure E2A), albeit with less frequency (~30% of mice) and in lesser abundance. The histology and BALF cytospins of ASM-HT mice were similar to those of WT mice. In concordance with histological findings, the Western blot analysis of whole lung lysates demonstrated markedly increased Ym1/2 protein in ASMKO lungs compared with WT lungs (Figure 1C).

Spontaneous Recruitment of Inflammatory Cells to the ASMKO Lungs

We next evaluated whether ASMKO mice had alterations in macrophage subsets or other cellular markers of lung inflammation. We first examined BALF, and, as previously reported (6, 33), we noted an overall increased number of macrophages, neutrophils, and lymphocytes in the BALF cytospins of ASMKO compared with WT mice (Figure 2A), suggestive of a spontaneous inflammatory response. The cell composition of BALF in ASM-HT mice was similar to that in WT mice (Figure 2A). Immunophenotyping of BALF by flow cytometry indicated that in WT mice, lung macrophages ($CD45^+/Ly6G^-/Ly6C^-/F480^+/CD64^+$) were comprised almost exclusively of $CD11c^+/CD11b^-$ cells, representing resident airspace (alveolar) macrophages (Figures 2B and 2C). In contrast, in the BALF from ASMKO mice, we noted a new population (10% of total macrophages) of $CD11c^{+/-}/CD11b^+$ monocyte-derived recruited macrophages (Figures 2B and 2C). In ASMKO mice, both $CD11c^+/CD11b^-$ macrophages and $CD11c^{+/-}/CD11b^+$ macrophages exhibited much broader light scatter than WT macrophages (Figures 2C and E3), consistent with the increased size and granularity noted on histology.

We next studied cell suspensions from whole lungs that were not subjected to BAL to characterize the entire lung macrophage population ($CD45^+/CD64^+/MerTK^+$). We used CD11c and Siglec F (SigF) markers to define $SigF^+/CD11c^+$, $SigF^-/CD11c^+$, and $SigF^-/CD11c^-$ macrophage populations (Figure 3A). As expected, in WT mice, ~93% of the lung macrophages were $SigF^+/CD11c^+$ (Figures 3A and 3B), with the remaining 7% being $CD11b^+$ comprising $SigF^-/CD11c^-$ cells with sparse $SigF^-/CD11c^+$ cells. The macrophage populations in ASM-HT mice closely resembled those in WT mice. In contrast, the lung macrophages in ASMKO mice comprised fewer $SigF^+/CD11c^+$ cells (~58%), with marked increases in $SigF^-/CD11c^-$ (19%) and $SigF^-/CD11c^+$ (22%) cells, suggesting recruitment and maturation of monocyte-derived macrophages, respectively. The $CD11c^-/SigF^-$ population was $Ly6C^-$ (Figure E1D), indicating that these cells are not monocytes. Moreover, the $SigF^+/CD11c^+$ macrophages in ASMKO mice had increased CD11b levels, suggesting a proinflammatory phenotype. The forward and side light scatter of all three macrophage populations was markedly increased in ASMKO mice compared with WT mice (Figures 3C and E4), consistent with increased size and granularity also noted on lung histology. Similar to findings noted in the BALF, neutrophils tended to be increased in ASMKO lungs (Figure E4).

Markers of Inflammation in ASMKO Mice

We investigated whether the increased inflammatory cells in ASMKO lungs were associated with other inflammatory biomarkers, and we used a customized MSD panel assay to measure concentrations of select cytokines in plasma and lung tissue. Compared with WT or ASM-HT mice, proinflammatory cytokines were increased in ASMKO mice by approximately twofold in the plasma and by an even higher magnitude in the lung (TNF-α: 2.2-fold plasma and 3.5-fold lung, IL-6: 2.7-fold plasma and 5.6-fold lung, KC/GRO: 2.1-fold plasma and 4.0-fold lung, IL-1β: not detected in the plasma and 2.7-fold lung, and IL-5: 1.9-fold plasma and 2.8-fold lung) (Figure 4; absolute cytokine concentrations in Figure E5). IL-4 concentrations were below the detection limit in the plasma of all animals but were detectable in the lung tissue of ~70% of ASMKO mice, significantly more than in WT mice (Figures 4 and Figures E5A and E5B). There were no differences between ASMKO and WT mice in the plasma and lungs concentrations of the antiinflammatory cytokine IL-10. These results indicate that the absence of ASM leads to the activation of several inflammatory pathways not only in the lungs but also systemically.

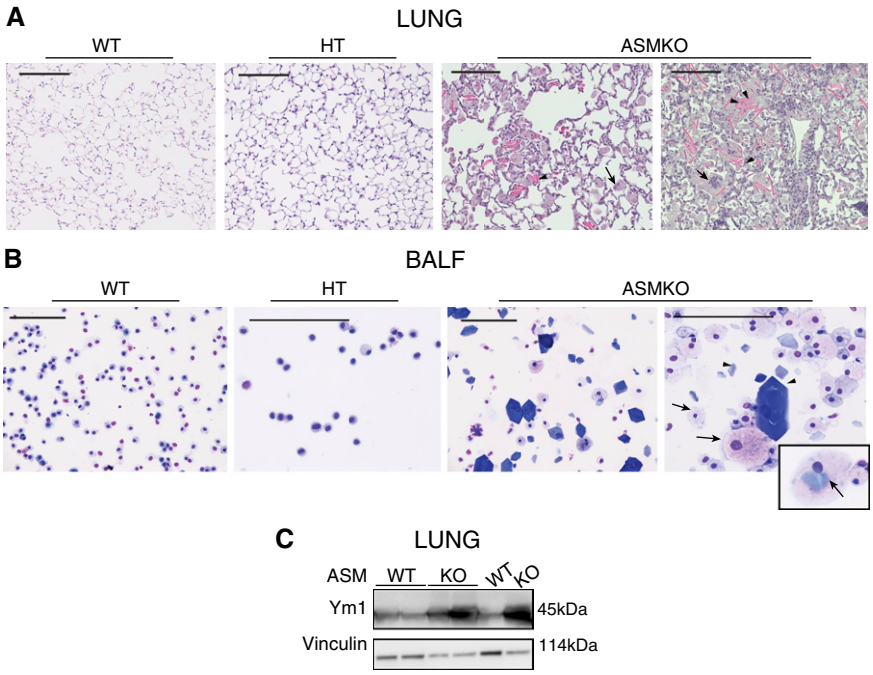

Figure 1. Lung histology in ASM (acid sphingomyelinase)-knockout (KO) homozygous (ASMKO; *Smpd*$^{-/-}$) mice. (*A*) Hematoxylin and eosin–stained sections of lungs. Arrows: enlarged, lipid-laden macrophages (foamy cells) in ASMKO lung. Arrowheads: eosinophilic crystalline inclusions. Scale bars, 100 μm. (*B*) BAL fluid (BALF) cytospins stained with Diff-Quick Stain (Wright-Giemsa). Arrows: enlarged macrophages in ASMKO BALF. Arrowheads: polygonal crystals. Scale bars, 100 μm. (*C*) Western blot of Ym1 in lung tissue lysates; vinculin was used as loading control. HT = ASM heterozygous (*Smpd*$^{+/-}$); WT = wild type (*Smpd*$^{+/+}$).

Cellular Localization of Ym1 Protein in ASMKO Lungs

Typically, Ym1 is expressed by resident airspace macrophages and portends an "M2"-like macrophage phenotype. Because we found markedly elevated Ym1 concentrations concurrently with new populations of macrophages in ASMKO lungs, we next determined which macrophage populations in ASMKO lungs harbor Ym1. Using flow cytometry, we found that in WT mice, Ym1 was present exclusively in SigF^{+}/CD11c^{+} macrophages (Figure 5A), undetectable in interstitial (SigF^{-}/CD11c^{-}) CD11b^{+} cells, and not evaluable in SigF^{-}/CD11c^{+} because of their low number. In the ASMKO mice, SigF^{+}/CD11c^{+} macrophages also expressed Ym1, but because of high cellular autofluorescence, its quantification was unreliable and therefore not directly comparable with the Ym1 concentrations in WT mice. However, in striking contrast to WT mice, both SigF^{-}/CD11c^{-} and SigF^{+}/CD11c^{+} macrophages in ASMKO mice were highly positive for Ym1. Because Ym1 may be produced by other cell types, including neutrophils and eosinophils, we evaluated Ym1 concentrations in Ly6G^{+}/CD11b^{+} (neutrophil markers) and CD64^{-}/SigF^{+}/CD11c^{-}/CD11b^{+} (eosinophil markers) cells. In comparison with WT mice, the Ym1 expression in ASMKO mice was appreciably lower in neutrophils and higher in eosinophils (Figure 5A). Furthermore, nonhematopoietic, CD45^{-} cells, which lacked Ym1 staining in WT mice, were highly Ym1-positive in ASMKO mice. These data were complemented by immunofluorescence microscopy that showed that in WT mice, only CD11c^{+} cells were positive for Ym1 (Figure 5B), whereas in ASMKO mice, both CD11c^{+} and CD11b^{+} stained for Ym1 (Figure 5B). In addition, ASMKO lungs harbored giant cells that stained positive for Ym1, and rather than staining positive for CD68, CD11b (Figure 5C), or CD11c (not shown), they costained positive for Ly6G (Figure 5C).

Macrophage Autophagy and Phagocytic Function in ASMKO Mice

Given the cellular inflammatory changes in the lungs of ASMKO mice, with high concentrations of Ym1 and crystal formation, we next evaluated the functional status of lung macrophages in these mice. ASMKO mice have a lysosomal storage disease and evidence of lysosome dysfunction. Indeed, we have recently shown that ASM inhibition triggers lysosomal autophagy and increase autophagy markers in ASMKO lungs (18). We recapitulated these results, using Western blotting of whole lung lysates, noting increased concentrations of autophagy markers p62 and LC3B and lysosomal marker LAMP2 in ASMKO lungs when compared with WT lungs (Figure 6A). Because there is an inverse relationship between amounts of autophagy and macrophage phagocytic function, in particular engulfment of opsonized targets (34), we focused our functional studies on Fc receptor-mediated phagocytosis and compared it with that of apoptotic cell clearance (efferocytosis) by lung macrophages in ASMKO mice. Because the macrophages' functional phenotype is highly impacted by their environment, we performed these assays *in vivo* by instillation of tagged phagocytic or efferocytosis targets into the lungs of mice, allowing for phagocytosis to occur *in situ*, followed by recovery and evaluation of lung macrophages. To evaluate Fc-dependent phagocytosis, we instilled Fc-coated fluorescent beads into the lungs of WT or ASMKO mice, recovered the macrophages by BAL after 4 hours, and used flow cytometry to assess the proportion of macrophages that had engulfed fluorescent beads. The phagocytic function in macrophages was significantly reduced (by 75%) in ASMKO mice compared with WT mice (Figure 6B). To evaluate macrophage efferocytosis, we introduced fluorescently labeled apoptotic thymocytes into the lungs of WT or ASMKO mice, recovered the macrophages by BAL after 1 hour, and measured the proportion of macrophages that had engulfed apoptotic cells using flow cytometry. In contrast to the significant reduction in phagocytosis of Fc-coated beads, ASMKO macrophages retained robust efferocytosis (Figure 6C).

Lipid Profiles in the Lungs of ASMKO Mice

We have previously shown that increased ceramide concentrations inhibit efferocytosis in both peripheral blood monocyte-derived and lung macrophages (18, 35). In turn, decreased S1P

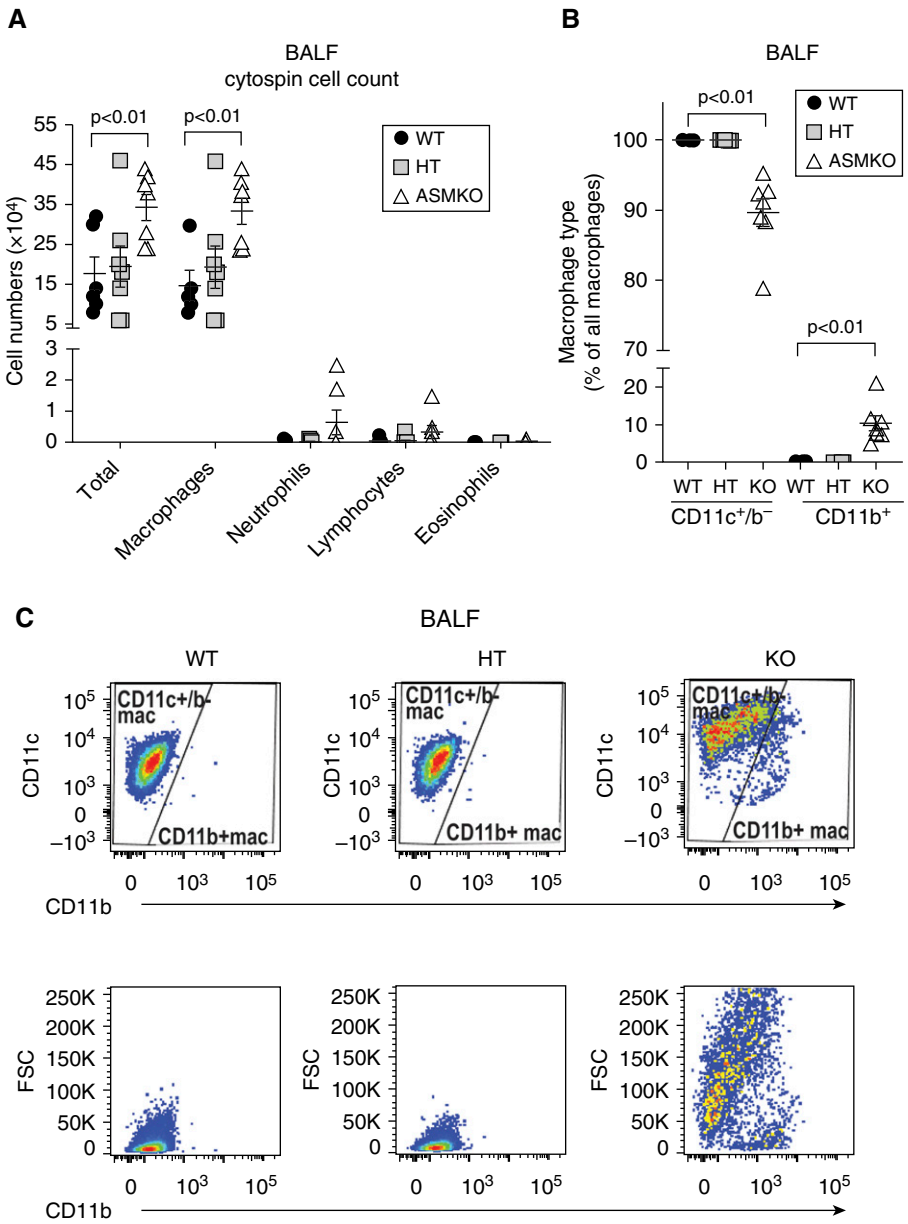

Figure 2. Inflammatory cells in the BALF of ASMKO mice. (*A*) Dot plot with mean abundance of inflammatory cell types in the BALF of WT, ASM-HT, and ASMKO mice determined by cell counts in BALF cytospins (mean ± SEM; $n = 6$–7/group; *t* test with Holm-Sidak correction for multiple comparisons). (*B*) Dot plot of relative abundance (percentage of all macrophages) of $CD11c^+/CD11b^-$ and $CD11b^+$ macrophages in BALF, measured by flow cytometry and identified as indicated in *C*, the CD11b versus CD11c plot. Each dot represents an individual mouse. Mean ± SEM; $n = 6$–7/group; Mann-Whitney test. (*C*) Representative flow cytometry graphs of the macrophage population in BALF of WT, ASM-HT, and ASMKO mice. Graphs are gated on the macrophage population defined as $CD45^+/Ly6G^-/Ly6C^-/F480^+/CD64^+$ in WT, ASM-HT, and ASMKO mice, with the top panels showing CD11b versus CD11c and the bottom panels showing CD11b versus FSC. FSC = forward scatter.

(sphingosine-1-phosphate) concentrations may stimulate efferocytosis of lung neutrophils (36). We next determined whether these lipid changes in ASMKO mice are congruent with functional alterations in phagocytosis and efferocytosis. ASM deficiency is expected to inhibit the hydrolysis of sphingomyelin to ceramide, therefore increasing sphingomyelin and decreasing ceramide concentrations. However, changes in sphingolipid metabolism can be rapidly compensated by other enzymes in the pathway, whereas the longstanding accumulation of sphingomyelin may itself alter cellular metabolism. Indeed, compared with WT mice, sphingomyelin concentrations were markedly increased (by approximately threefold and ~100-fold) in both the lung tissue and the BALF of ASMKO mice, respectively (Figures 7A and 7B). However, ceramide concentrations were unchanged in ASMKO lungs (Figure 7A) and were unexpectedly increased in the BALF (Figure 7B). In turn, ASMKO mice had markedly reduced S1P concentrations in the lung (Figure 7A). To our surprise, the BALF contained increased S1P concentrations in ASMKO mice (Figure 7B). We therefore inquired whether lipids are nonspecifically increased in the BALF of ASMKO mice. That appeared indeed to be the case, as lysophosphatidylcholine concentrations were also higher in the BALF of ASMKO mice (Figure E6A), whereas its downstream metabolite, lysophosphatidic acid (LPA), was reduced in the lung tissue (Figure E6B).

Discussion

We report novel aspects of NPD-associated lung pathology that, in addition to recruitment of neutrophils and monocyte-derived macrophages, include accumulation of eosinophilic crystals and a complex pattern of local and systemic inflammation. Both resident and recruited macrophages found in airspaces contained high concentrations of Ym1, an enzymatically inactive chitinase-like protein associated with "M2-" or alternative activation of macrophages. Indeed, ASMKO macrophages were deficient in Fc-mediated phagocytosis but exhibited robust efferocytosis and activation of autophagy.

We demonstrate for the first time that ASM is implicated in the determination of lung macrophage subset abundance and function. Previous studies of ASMKO mice demonstrated age-dependent increased abundance of lung macrophages, including enlarged, lipid-laden (foamy) macrophages as well as neutrophil recruitment associated with the secretion of monocyte and neutrophil chemoattractant cytokines MIP-1a and MIP-2 (6). We provide a deeper phenotyping of lung macrophages in these mice, demonstrating that in sharp

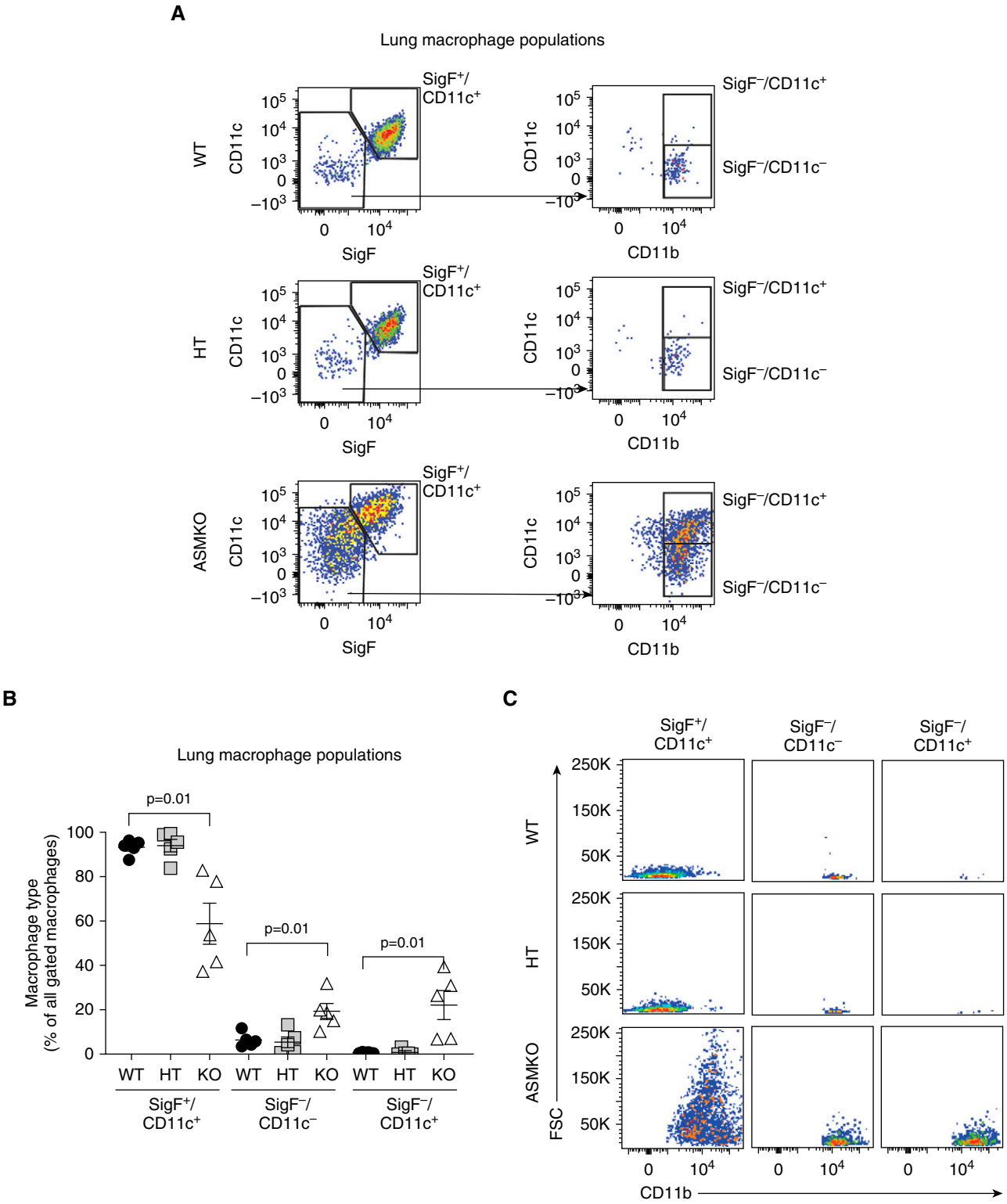

Figure 3. Macrophage populations in the lung tissue of ASMKO mice. (*A*) Flow cytometry plots depicting the gating strategy used to define macrophage populations in single-cell suspensions derived from lung digestions from WT, ASM-HT, and ASMKO mice. Graphs are gated on the total macrophage population, defined as $CD45^+/CD64^+/MerTK^+$. Neutrophils and eosinophils were excluded from this gate. (*B*) Dot plot of relative abundance (percentage of all gated macrophages) of $SigF^+/CD11c^+$, $SigF^-/CD11c^-$, and $SigF^-/CD11c^+$ macrophage populations in single-cell suspension from lungs of WT, ASM-HT, and ASMKO determined by flow cytometry (mean ± SEM; $n = 5$/group; *t* test). (*C*) Representative plots of macrophage populations in WT, ASM-HT, and ASMKO lung single-cell suspensions. All panels depict CD11b versus FSC.

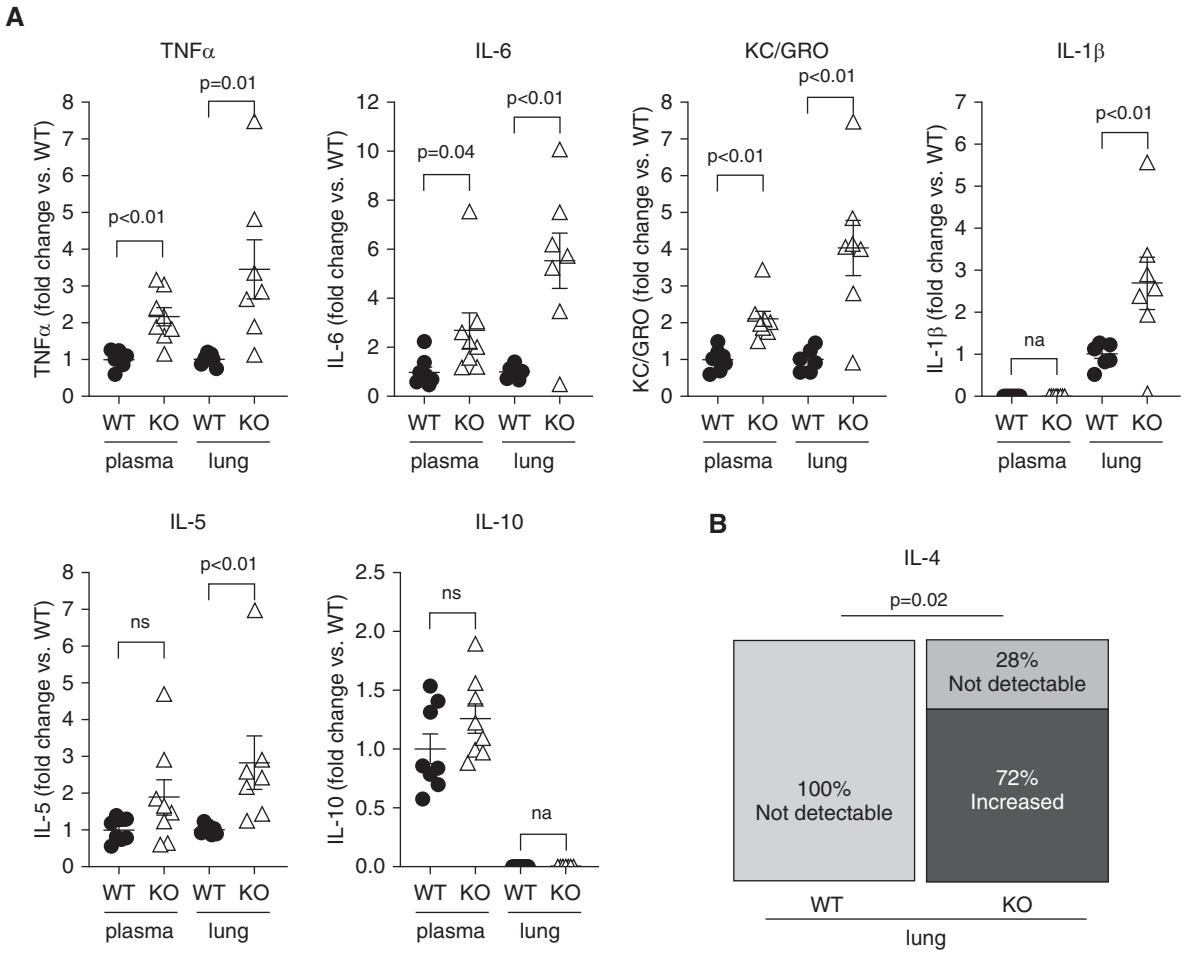

Figure 4. Proinflammatory cytokines in plasma and lung of ASMKO mice. (*A*) Dot plots with relative concentrations of the indicated cytokines in the plasma and lung tissue lysate of WT and ASMKO mice, measured by a custom Meso Scale Discovery panel electrochemiluminescence assay. Cytokine concentrations in plasma or lung were normalized to the average of the respective WT control samples. Mean ± SEM; $n = 7–8$/group; *t* test. (*B*) Pie charts with relative *n* (%) of animals with increased lung concentrations of IL-4 ($n = 7$/group; $P = 0.02$; Fisher's exact test, two-tailed). GRO = human growth-regulated oncogene; KC = keratinocyte chemoattractant; na = not available because of values below the quantitation range of the assay; ns = not significant.

distinction to WT and ASM-HT mice, in which the majority population consists of resident interstitial and airspace macrophages (26, 37), the increased number of macrophages in ASMKO mice was largely accounted for by recruited $CD11b^{+}$ cells. These macrophages were large and granular, and they exhibited a continuum of CD11c expression and included a subpopulation with Siglec F positivity. Because CD11c expression reflects lung residence, the wide range of CD11c expression suggests ongoing recruitment of monocyte-derived macrophages to the lung. Macrophages with the highest CD11c expression also displayed Siglec F, a marker for self-renewing embryonic airspace macrophages that can also be progressively acquired by recruited macrophages that persist in the lung environment (26, 38). Thus, in ASMKO mice, the $CD11c^{+}/SigF^{+}$ macrophage population may comprise monocyte-derived recruited macrophages that have been reprogrammed to resident airspace phenotype and the bona-fide embryonic-derived resident airspace macrophages. Absent lineage tracing, the relative contribution of these two populations cannot be precisely determined.

The typical framing of macrophage activation within the M1/M2 polarization paradigm is more complex *in vivo* (39), where lung macrophages coexpress M1 and M2 markers during health and inflammation (26, 40). The functional phenotype of the ASMKO lung macrophages had features of M2 alternative activation, given the presence of Ym1 among all subpopulations with robust efferocytosis and decreased Fc-mediated phagocytosis. However, proinflammatory cytokines were also markedly increased in the lungs, suggesting concomitant M1 classical activation. Although the lysosomal storage defect in ASMKO mice may be responsible for this complex macrophage activation, a potential role for excessive Ym1 accumulation and crystal formation is intriguing. Ym1 is a lectin-like chitinase devoid of enzymatic activity expressed by resident airspace macrophages and neutrophils (19–21). Transient elevations of Ym1 expression in macrophages, neutrophils, and $Ly6C^{Hi}$ monocytes are noted during injury repair (31, 41–43),

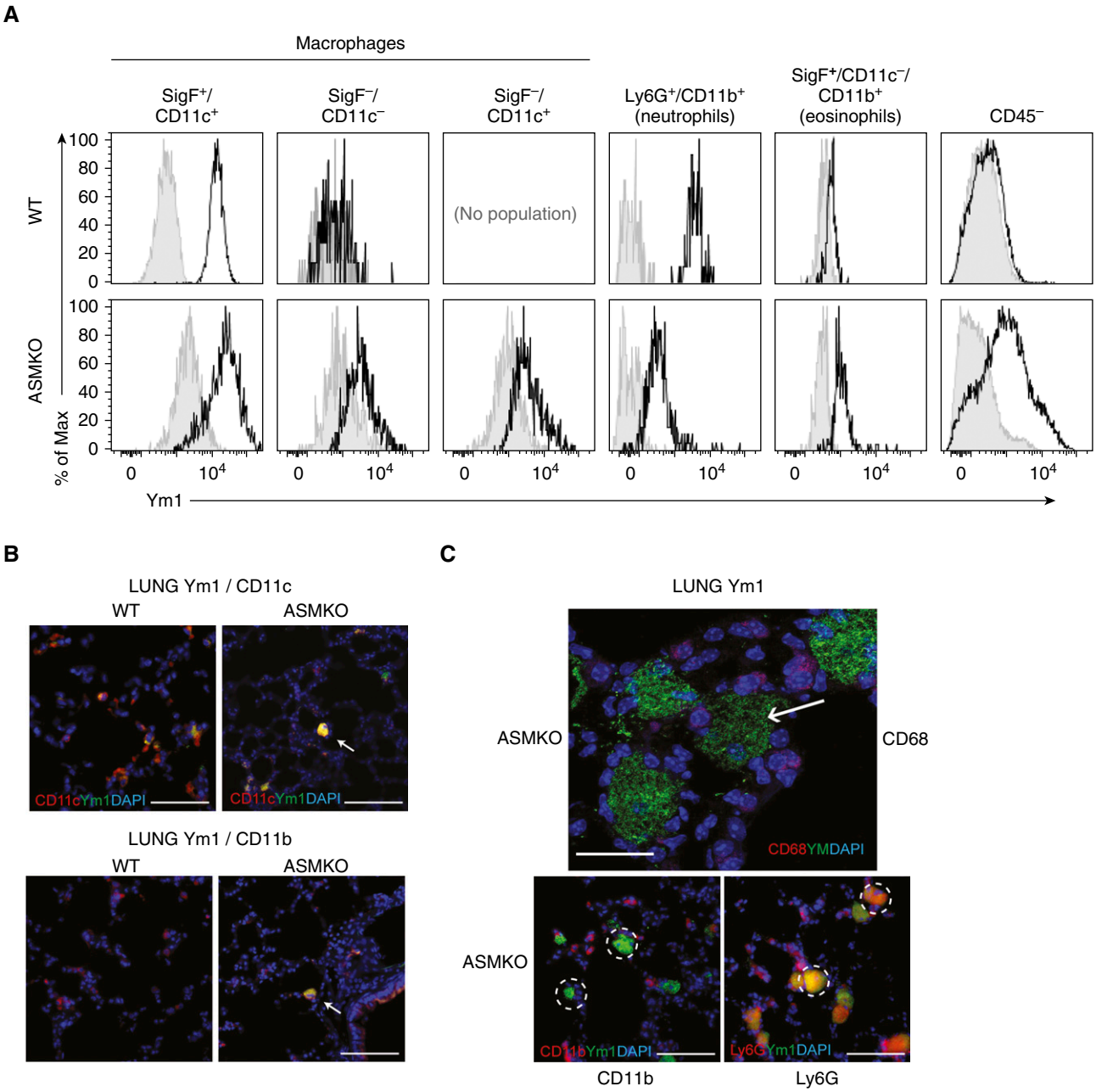

Figure 5. Association of Ym1 with inflammatory cells in the lungs of ASMKO mice. (*A*) Representative flow cytometry histograms of Ym1 levels in the indicated populations in whole lung single-cell suspension in WT and ASMKO mice. Ym1 (black histograms) levels (*x*-axis) are expressed relative to the number of cells (*y*-axis, percentage of maximum cells). Gray histograms show control without Ym1 antibody and "no population" indicates there were too few cells to form a histogram. (*B* and *C*) Representative immunofluorescence images of mouse lung sections ($n = 3$) showing costaining of Ym1/2 (green) and nuclei (DAPI, blue) with (*B*) CD11c (red, top), CD11b (red, bottom) in WT and ASMKO mice or with (*C*) CD68, CD11b, or Ly6G (all red) in ASMKO mice. *Note,* within dashed circles are giant cellular conglomerates that are only present in ASMKO mice and have intense Ym1 and Ly6G staining but lack staining for CD68, CD11b, or CD11b. Arrows indicate foamy macrophages that have high expressions of CD11b, CD11c, and Ym1. Scale bars, 100 μm.

whereas persistent lung elevations have been noted in Th2 inflammatory conditions (e.g., parasitic infections or allergic asthma) (44–48). Excessive Ym1 and crystallization similar to that in ASMKO mice have been described during neutrophilic inflammation in chronic granulomatous disease (31) or eosinophilic crystalline pneumonia (32) in mice. In the ASMKO mice, all macrophage subsets expressed Ym1 protein, as did eosinophils, neutrophils, and noninflammatory cells. However, given the lack of granulomatous lung inflammation and the modest lung amounts of neutrophilic or eosinophilic inflammation,

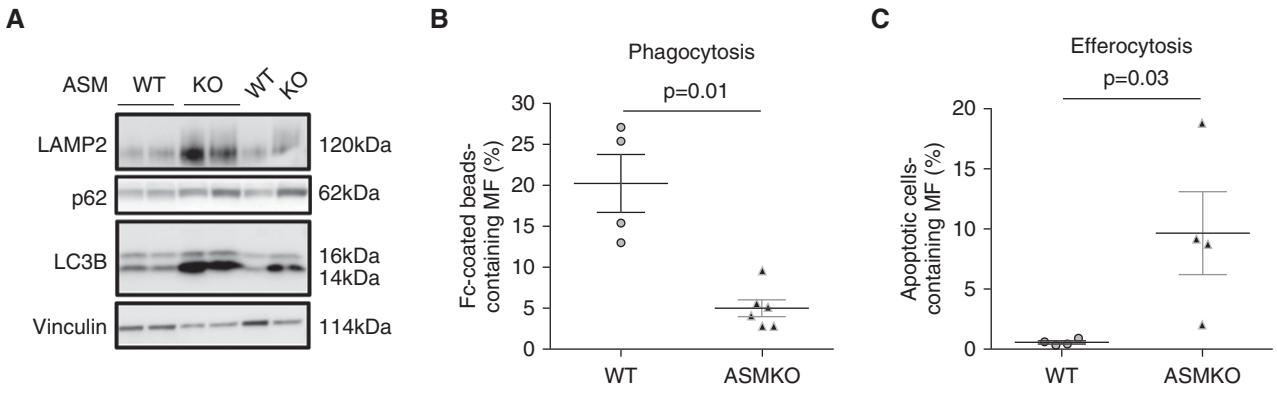

Figure 6. Lung macrophage function in ASMKO mice. (*A*) Lysosomal autophagy markers detected by Western blot of lung tissue homogenates. Vinculin was used as a loading control. (*B*) *In vivo* phagocytosis by airspace macrophages. Dot plot showing the relative abundance of airspace macrophages (percentage of total macrophages in BALF) that engulfed fluorescently labeled Fc-coated beads instilled (1×10^6/mouse, 4 h) into the lungs of mice and assessed by flow cytometry. Mean ± SEM; $n = 4$–6/group; $P = 0.01$; Mann-Whitney test. (*C*) *In vivo* efferocytosis by airspace macrophages. Dot plot showing the relative abundance of airspace macrophages (percentage of total macrophages in BALF) that engulfed apoptotic mouse thymocytes instilled (1×10^6/mouse, 1 h) into the lungs of mice and analyzed by flow cytometry. Mean ± SEM; $n = 4$/group; $P = 0.02$; Mann-Whitney test.

we speculate that the crystalopathy of ASMKO mice may be driven by a defect in macrophage phagocytosis and lysosomal dysfunction that impairs the ability of lung macrophages to engulf and clear Ym1/2 crystals despite increased autophagy. It remains to be proven whether Ym1 crystals in ASMKO mice are responsible for the secretion of the Th2 (IL-4 and IL-5) or Th1 proinflammatory cytokines. Of note, Charcot-Leyden crystals in human asthma, which are similar in shape to the Ym1

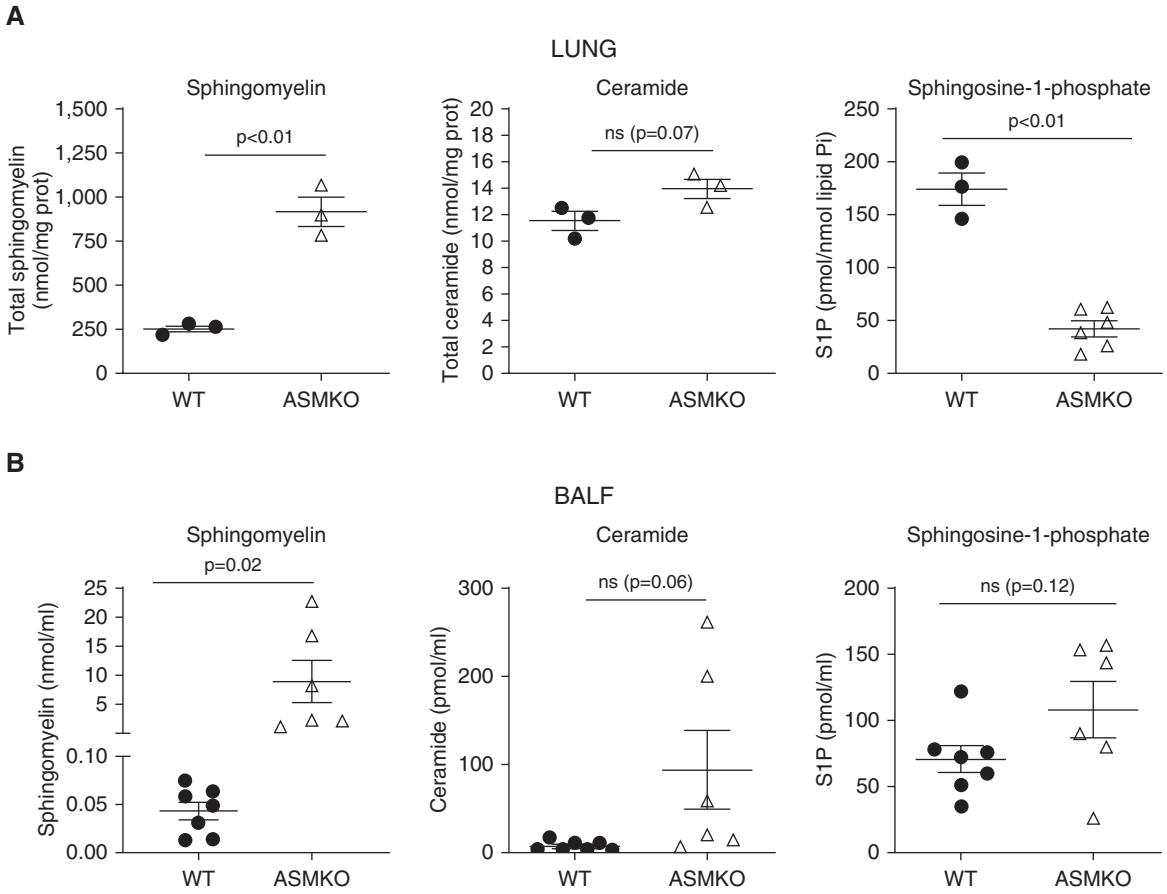

Figure 7. Sphingolipid concentrations in ASMKO mice. (*A*) Comparisons of indicated sphingolipid concentrations in lungs of WT versus ASMKO mice. Each point represents an individual animal. Mean ± SEM; $n = 3$–6/group; Student's *t* test. (*B*) Comparison of indicated sphingolipid concentrations in the BALF of WT versus ASMKO mice. Each point represents an individual animal. Mean ± SEM; $n = 6$–7/group; Student's *t* test.

crystals but are composed from a different protein (galectin-10), were sufficient to drive a Th2 response (49).

As expected, ASM deficiency led to sphingomyelin accumulation, which is known to occur in all cell types, including macrophages (3, 50). Furthermore, because ASM and ceramidase activities are coupled (18), the downstream production of sphingosine, S1P, as well as that of other bioactive lipids may be affected in ASMKO mice. Indeed, ASMKO lungs exhibited significantly reduced S1P and LPA concentrations, which may impact a multitude of biological activities, including autophagy. In particular, the loss of the stimulatory effect of S1P on mTOR (51, 52), combined with the autophagy inhibitory effect of LPA, might provide a permissive signaling environment for autophagy noted in ASMKO mice. Although autophagy may affect macrophage engulfment, given the opposite impact of ASM deficiency on Fc-mediated efferocytosis and phagocytosis, it is likely that the latter may involve other mechanisms. Elucidation of these may also help explain the defective receptor-mediated uptake (53) and processing and clearance of surfactant phospholipids by macrophages (54) in ASMKO mice.

Although our focus here was on lung macrophage function, the contribution of structural cells abnormalities such as epithelial and endothelial cells or fibroblasts to NPD pathobiology cannot be ignored. For example, ASM knockdown in human lung epithelial cells was sufficient to increase their secretion of proinflammatory cytokines such as IL-8 (55). Injury or activation of epithelial cells in ASM deficiency could itself stimulate inflammatory cell accumulation. In addition, the functional changes in engulfment could be due to a cell-autonomous phenotype change in ASMKO resident alveolar macrophages or could be a result of the contribution of the recruited macrophages. Elucidation of which cell type drives inflammation in ASMKO mice will have to be determined by future experiments using cell-specific deletion or inhibition of *Smpd1*.

Respiratory involvement is present in 75% of patients with NPD and, together with liver failure, represents the most common cause of death (56–58). The marked impairment of Fc-mediated phagocytosis in ASMKO mice may provide a mechanistic insight into the increased frequency of respiratory infections reported in patients with NPD (5, 59). Furthermore, the Th2 and the M2 inflammatory phenotypes in ASMKO mice are respective drivers of asthma and lung fibrosis, known manifestations of lung disease in NPD (4, 60–62). However, there are limitations of ASMKO mice as a model of NPD lung disease, in that these animals do not develop lung fibrosis. Also, human NPD lungs have not been reported to feature crystalopathy, although they do exhibit proteinaceous material in the airspaces and increased chitotriosidase activity, an enzyme involved in chitin breakdown, which was proposed as disease biomarker (63–65). Therefore, even if the Ym1 crystalopathy is unique to the mouse model, it would be interesting to query whether equivalent lectin-like structures may be present in human lungs. Finally, the lack of inflammatory changes in the partial ASM deficiency (ASM-HT) suggests the possibility that restoring sphingomyelin hydrolysis could prevent lung changes noted herein.

In conclusion, genetic ASM deficiency is associated with marked changes in lung macrophage specification and macrophage dysfunction, with deficient Fc-mediated phagocytosis, crystal-associated neutrophilic and monocyte recruitment, and a mixed Th2 and Th1 response. These findings may have importance in understanding the pathogenesis of NPD- and other crystal-associated lung diseases. ■

Author disclosures are available with the text of this article at www.atsjournals.org.

References

1. McGovern MM, Avetisyan R, Sanson BJ, Lidove O. Disease manifestations and burden of illness in patients with acid sphingomyelinase deficiency (ASMD). *Orphanet J Rare Dis* 2017;12:41.
2. Minai OA, Sullivan EJ, Stoller JK. Pulmonary involvement in Niemann-Pick disease: case report and literature review. *Respir Med* 2000;94: 1241–1251.
3. Schuchman EH, Desnick RJ. Types A and B Niemann-Pick disease. *Mol Genet Metab* 2017;120:27–33.
4. Chebib N, Thivolet-Bejui F, Cottin V. Interstitial lung disease associated with adult Niemann-Pick disease type B. *Respiration* 2017;94:237–238.
5. von Ranke FM, Pereira Freitas HM, Mançano AD, Rodrigues RS, Hochhegger B, Escuissato D, *et al*. Pulmonary involvement in Niemann-Pick disease: a state-of-the-art review. *Lung* 2016;194:511–518.
6. Dhami R, He X, Gordon RE, Schuchman EH. Analysis of the lung pathology and alveolar macrophage function in the acid sphingomyelinase-deficient mouse model of Niemann-Pick disease. *Lab Invest* 2001;81:987–999.
7. Horinouchi K, Erlich S, Perl DP, Ferlinz K, Bisgaier CL, Sandhoff K, *et al*. Acid sphingomyelinase deficient mice: a model of types A and B Niemann-Pick disease. *Nat Genet* 1995;10:288–293.
8. Otterbach B, Stoffel W. Acid sphingomyelinase-deficient mice mimic the neurovisceral form of human lysosomal storage disease (Niemann-Pick disease). *Cell* 1995;81:1053–1061.
9. Schissel SL, Schuchman EH, Williams KJ, Tabas I. Zn2+-stimulated sphingomyelinase is secreted by many cell types and is a product of the acid sphingomyelinase gene. *J Biol Chem* 1996;271:18431–18436.
10. Grassmé H, Cremesti A, Kolesnick R, Gulbins E. Ceramide-mediated clustering is required for CD95-DISC formation. *Oncogene* 2003;22: 5457–5470.
11. Grassme H, Jekle A, Riehle A, Schwarz H, Berger J, Sandhoff K, *et al*. CD95 signaling via ceramide-rich membrane rafts. *J Biol Chem* 2001; 276:20589–20596.
12. Smith EL, Schuchman EH. The unexpected role of acid sphingomyelinase in cell death and the pathophysiology of common diseases. *FASEB J* 2008;22:3419–3431.
13. Truman JP, Al Gadban MM, Smith KJ, Hammad SM. Acid sphingomyelinase in macrophage biology. *Cell Mol Life Sci* 2011;68:3293–3305.
14. Paris F, Fuks Z, Kang A, Capodieci P, Juan G, Ehleiter D, *et al*. Endothelial apoptosis as the primary lesion initiating intestinal radiation damage in mice. *Science* 2001;293: 293–297.
15. Santana P, Peña LA, Haimovitz-Friedman A, Martin S, Green D, McLoughlin M, *et al*. Acid sphingomyelinase-deficient human lymphoblasts and mice are defective in radiation-induced apoptosis. *Cell* 1996;86:189–199.
16. García-Ruiz C, Colell A, Marí M, Morales A, Calvo M, Enrich C, *et al*. Defective TNF-alpha-mediated hepatocellular apoptosis and liver damage in acidic sphingomyelinase knockout mice. *J Clin Invest* 2003;111:197–208.
17. Fowler S. Lysosomal localization of sphingomyelinase in rat liver. *Biochim Biophys Acta* 1969;191:481–484.
18. Justice MJ, Bronova I, Schweitzer KS, Poirier C, Blum JS, Berdyshev EV, *et al*. Inhibition of acid sphingomyelinase disrupts LYNUS signaling and triggers autophagy. *J Lipid Res* 2018;59: 596–606.

19. Hussell T, Bell TJ. Alveolar macrophages: plasticity in a tissue-specific context. *Nat Rev Immunol* 2014;14:81–93.
20. Raes G, Van den Bergh R, De Baetselier P, Ghassabeh GH, Scotton C, Locati M, *et al*. Arginase-1 and Ym1 are markers for murine, but not human, alternatively activated myeloid cells. *J Immunol* 2005;174: 6561; author reply 6561–6562.
21. Svedberg FR, Brown SL, Krauss MZ, Campbell L, Sharpe C, Clausen M, *et al*. The lung environment controls alveolar macrophage metabolism and responsiveness in type 2 inflammation. *Nat Immunol* 2019;20:571–580.
22. Byrne AJ, Mathie SA, Gregory LG, Lloyd CM. Pulmonary macrophages: key players in the innate defence of the airways. *Thorax* 2015;70: 1189–1196.
23. Duan M, Li WC, Vlahos R, Maxwell MJ, Anderson GP, Hibbs ML. Distinct macrophage subpopulations characterize acute infection and chronic inflammatory lung disease. *J Immunol* 2012;189: 946–955.
24. Duan M, Steinfort DP, Smallwood D, Hew M, Chen W, Ernst M, *et al*. CD11b immunophenotyping identifies inflammatory profiles in the mouse and human lungs. *Mucosal Immunol* 2016;9:550–563.
25. Johnston LK, Rims CR, Gill SE, McGuire JK, Manicone AM. Pulmonary macrophage subpopulations in the induction and resolution of acute lung injury. *Am J Respir Cell Mol Biol* 2012;47:417–426.
26. Mould KJ, Barthel L, Mohning MP, Thomas SM, McCubbrey AL, Danhorn T, *et al*. Cell origin dictates programming of resident versus recruited macrophages during acute lung injury. *Am J Respir Cell Mol Biol* 2017;57:294–306.
27. Koike K, Beatman EL, Schweitzer KS, Justice MJ, Mikosz AM, Ni K, *et al*. Subcutaneous administration of neutralizing antibodies to endothelial monocyte-activating protein II attenuates cigarette smoke-induced lung injury in mice. *Am J Physiol Lung Cell Mol Physiol* 2019;316:L558–L566.
28. Zhang X, Goncalves R, Mosser DM. The isolation and characterization of murine macrophages. *Curr Protoc Immunol* 2008;Chapter 14:Unit 14.1.
29. Berdyshev EV, Gorshkova IA, Usatyuk P, Zhao Y, Saatian B, Hubbard W, *et al*. De novo biosynthesis of dihydrosphingosine-1-phosphate by sphingosine kinase 1 in mammalian cells. *Cell Signal* 2006;18: 1779–1792.
30. Guo L, Johnson RS, Schuh JC. Biochemical characterization of endogenously formed eosinophilic crystals in the lungs of mice. *J Biol Chem* 2000;275:8032–8037.
31. Harbord M, Novelli M, Canas B, Power D, Davis C, Godovac-Zimmermann J, *et al*. Ym1 is a neutrophil granule protein that crystallizes in p47phox-deficient mice. *J Biol Chem* 2002;277: 5468–5475.
32. Hoenerhoff MJ, Starost MF, Ward JM. Eosinophilic crystalline pneumonia as a major cause of death in 129S4/SvJae mice. *Vet Pathol* 2006;43:682–688.
33. Böll S, Ziemann S, Ohl K, Klemm P, Rieg AD, Gulbins E, *et al*. Acid sphingomyelinase regulates T_H 2 cytokine release and bronchial asthma. *Allergy* 2020;75:603–615.
34. Jin L, Batra S, Jeyaseelan S. Deletion of Nlrp3 augments survival during polymicrobial sepsis by decreasing autophagy and enhancing phagocytosis. *J Immunol* 2017;198:1253–1262.
35. Petrusca DN, Gu Y, Adamowicz JJ, Rush NI, Hubbard WC, Smith PA, *et al*. Sphingolipid-mediated inhibition of apoptotic cell clearance by alveolar macrophages. *J Biol Chem* 2010;285:40322–40332.
36. Perez DA, Galvão I, Athayde RM, Rezende BM, Vago JP, Silva JD, *et al*. Inhibition of the sphingosine-1-phosphate pathway promotes the resolution of neutrophilic inflammation. *Eur J Immunol* 2019;49: 1038–1051.
37. Janssen WJ, Barthel L, Muldrow A, Oberley-Deegan RE, Kearns MT, Jakubzick C, *et al*. Fas determines differential fates of resident and recruited macrophages during resolution of acute lung injury. *Am J Respir Crit Care Med* 2011;184:547–560.
38. Gibbings SL, Goyal R, Desch AN, Leach SM, Prabagar M, Atif SM, *et al*. Transcriptome analysis highlights the conserved difference between embryonic and postnatal-derived alveolar macrophages. *Blood* 2015;126:1357–1366.
39. Mosser DM, Edwards JP. Exploring the full spectrum of macrophage activation. *Nat Rev Immunol* 2008;8:958–969.
40. Mould KJ, Jackson ND, Henson PM, Seibold M, Janssen WJ. Single cell RNA sequencing identifies unique inflammatory airspace macrophage subsets. *JCI Insight* 2019;4:e126556.
41. Cuartero MI, Ballesteros I, Moraga A, Nombela F, Vivancos J, Hamilton JA, *et al*. N2 neutrophils, novel players in brain inflammation after stroke: modulation by the PPARγ agonist rosiglitazone. *Stroke* 2013; 44:3498–3508.
42. Goren I, Pfeilschifter J, Frank S. Uptake of neutrophil-derived Ym1 protein distinguishes wound macrophages in the absence of interleukin-4 signaling in murine wound healing. *Am J Pathol* 2014; 184:3249–3261.
43. Ikeda N, Asano K, Kikuchi K, Uchida Y, Ikegami H, Takagi R, *et al*. Emergence of immunoregulatory Ym1 $^{+}$Ly6C^{hi} monocytes during recovery phase of tissue injury. *Sci Immunol* 2018;3:eaat0207.
44. Nair MG, Gallagher IJ, Taylor MD, Loke P, Coulson PS, Wilson RA, *et al*. Chitinase and Fizz family members are a generalized feature of nematode infection with selective upregulation of Ym1 and Fizz1 by antigen-presenting cells. *Infect Immun* 2005;73:385–394.
45. Shuhui L, Mok YK, Wong WS. Role of mammalian chitinases in asthma. *Int Arch Allergy Immunol* 2009;149:369–377.
46. Webb DC, McKenzie AN, Foster PS. Expression of the Ym2 lectin-binding protein is dependent on interleukin (IL)-4 and IL-13 signal transduction: identification of a novel allergy-associated protein. *J Biol Chem* 2001;276:41969–41976.
47. Welch JS, Escoubet-Lozach L, Sykes DB, Liddiard K, Greaves DR, Glass CK. TH2 cytokines and allergic challenge induce Ym1 expression in macrophages by a STAT6-dependent mechanism. *J Biol Chem* 2002;277:42821–42829.
48. Zhang L, Wang M, Kang X, Boontheung P, Li N, Nel AE, *et al*. Oxidative stress and asthma: proteome analysis of chitinase-like proteins and FIZZ1 in lung tissue and bronchoalveolar lavage fluid. *J Proteome Res* 2009;8:1631–1638.
49. Persson EK, Verstraete K, Heyndrickx I, Gevaert E, Aegerter H, Percier JM, *et al*. Protein crystallization promotes type 2 immunity and is reversible by antibody treatment. *Science* 2019;364:eaaw4295.
50. Schuchman EH. Acid sphingomyelinase, cell membranes and human disease: lessons from Niemann-Pick disease. *FEBS Lett* 2010;584: 1895–1900.
51. Liu G, Burns S, Huang G, Boyd K, Proia RL, Flavell RA, *et al*. The receptor S1P1 overrides regulatory T cell-mediated immune suppression through Akt-mTOR. *Nat Immunol* 2009;10:769–777.
52. Maeurer C, Holland S, Pierre S, Potstada W, Scholich K. Sphingosine-1-phosphate induced mTOR-activation is mediated by the E3-ubiquitin ligase PAM. *Cell Signal* 2009;21:293–300.
53. Dhami R, Schuchman EH. Mannose 6-phosphate receptor-mediated uptake is defective in acid sphingomyelinase-deficient macrophages: implications for Niemann-Pick disease enzyme replacement therapy. *J Biol Chem* 2004;279:1526–1532.
54. Ikegami M, Dhami R, Schuchman EH. Alveolar lipoproteinosis in an acid sphingomyelinase-deficient mouse model of Niemann-Pick disease. *Am J Physiol Lung Cell Mol Physiol* 2003;284: L518–L525.
55. MacFadden-Murphy E, Roussel L, Martel G, Bérubé J, Rousseau S. Decreasing SMPD1 activity in BEAS-2B bronchial airway epithelial cells results in increased NRF2 activity, cytokine synthesis and neutrophil recruitment. *Biochem Biophys Res Commun* 2017;482: 645–650.
56. Porta F, Pagliardini V, Barbera C, Calvo P, Pagliardini S, Lualdi S, *et al*. Neonatal chitotriosidase activity is not predictive for Niemann-Pick disease type A/B: implications for newborn screening for lysosomal storage disorders. *Mol Genet Metab* 2013;108:106.
57. Cassiman D, Packman S, Bembi B, Turkia HB, Al-Sayed M, Schiff M, *et al*. Corrigendum to "Cause of death in patients with chronic visceral and chronic neurovisceral acid sphingomyelinase deficiency (Niemann-Pick disease type B and B variant): literature review and report of new cases" [Mol. Genet. Metab. 118 (2016) 206-213]. *Mol Genet Metab* 2018;125:360.
58. Cassiman D, Packman S, Bembi B, Turkia HB, Al-Sayed M, Schiff M, *et al*. Cause of death in patients with chronic visceral and chronic neurovisceral acid sphingomyelinase deficiency (Niemann-Pick disease type B and B variant): literature review and report of new cases. *Mol Genet Metab* 2016;118:206–213.

59. Nicholson AG, Florio R, Hansell DM, Bois RM, Wells AU, Hughes P, *et al*. Pulmonary involvement by Niemann-Pick disease: a report of six cases. *Histopathology* 2006;48:596–603.
60. Bajaj S, Muranjan M, Karande S, Prabhat D. Rare disease heralded by pulmonary manifestations: avoiding pitfalls of an "asthma" label. *J Postgrad Med* 2017;63:122–127.
61. González-Reimers E, Sánchez-Pérez MJ, Bonilla-Arjona A, Rodríguez-Gaspar M, Carrasco-Juan JL, Alvarez-Argüelles H, *et al*. Case report: pulmonary involvement in an adult male affected by type B Niemann-Pick disease. *Br J Radiol* 2003;76:838–840.
62. Guillemot N, Troadec C, de Villemeur TB, Clément A, Fauroux B. Lung disease in Niemann-Pick disease. *Pediatr Pulmonol* 2007;42: 1207–1214.
63. De Castro-Orós I, Irún P, Cebolla JJ, Rodriguez-Sureda V, Mallén M, Pueyo MJ, *et al*.; Spanish NP-C Group. Assessment of plasma chitotriosidase activity, CCL18/PARC concentration and NP-C suspicion index in the diagnosis of Niemann-Pick disease type C: a prospective observational study. *J Transl Med* 2017;15:43.
64. Degtyareva AV, Proshlyakova TY, Gautier MS, Degtyarev DN, Kamenets EA, Baydakova GV, *et al*. Oxysterol/chitotriosidase based selective screening for Niemann-Pick type C in infantile cholestasis syndrome patients. *BMC Med Genet* 2019;20:123.
65. Voorink-Moret M, Goorden SMI, van Kuilenburg ABP, Wijburg FA, Ghauharali-van der Vlugt JMM, Beers-Stet FS, *et al*. Rapid screening for lipid storage disorders using biochemical markers: expert center data and review of the literature. *Mol Genet Metab* 2018;123:76–84.